Proceedings of the ASME 2014 Dynamic Systems and Control Conference
DSCC2014
October 22-24, 2014, San Antonio, TX, USA

DSCC2014-6207

SENSITIVITY COMPARISON TO LOOP LATENCIES BETWEEN DAMPING VERSUS STIFFNESS FEEDBACK CONTROL ACTION IN DISTRIBUTED CONTROLLERS

Ye Zhao
Human Centered Robotics Laboratory
Department of Mechanical Engineering
The University of Texas at Austin
Austin, Texas 78712
Email: yezhao@utexas.edu

Nicholas Paine
Human Centered Robotics Laboratory
Department of Mechanical Engineering
The University of Texas at Austin
Austin, Texas 78712
Email: npaine@utexas.edu

Luis Sentis
Human Centered Robotics Laboratory
Department of Mechanical Engineering
The University of Texas at Austin
Austin, Texas 78712
Email: lsentis@austin.utexas.edu

ABSTRACT

This paper studies the effects of damping and stiffness feedback loop latencies on closed-loop system stability and performance. Phase margin stability analysis, step response performance and tracking accuracy are respectively simulated for a rigid actuator with impedance control. Both system stability and tracking performance are more sensitive to damping feedback than stiffness feedback latencies. Several comparative tests are simulated and experimentally implemented on a real-world actuator to verify our conclusion. This discrepancy in sensitivity motivates the necessity of implementing embedded damping, in which damping feedback is implemented locally at the low level joint controller. A direct benefit of this distributed impedance control strategy is the enhancement of closed-loop system stability. Using this strategy, feedback effort and thus closed-loop actuator impedance may be increased beyond the levels possible for a monolithic impedance controller. High impedance is desirable to minimize tracking error in the presence of disturbances. Specially, trajectory tracking accuracy is tested by a fast swing and a slow stance motion of a knee joint emulating NASA-JSC's Valkyrie legged robot. When damping latencies are lowered beyond stiffness latencies, gravitational disturbance is rejected, thus demonstrating the accurate tracking performance enabled by a distributed impedance controller.

INTRODUCTION

In recent years, robotic task complexity has grown significantly. As one example, the disaster caused by the nuclear reactor meltdown of the Fukushima Daiichi power plant necessitated mobile robots be deployed to survey damage and assess danger levels [1]. However, simple tracked robots were the only available option, limiting the robotic capability to surveillance of areas accessible to a tracked, tethered vehicle. In response to this disaster, the United States DARPA research agency sponsored a competition, named the DARPA Robotics Challenge or DRC, requiring robots to be built to enter degraded human environments such

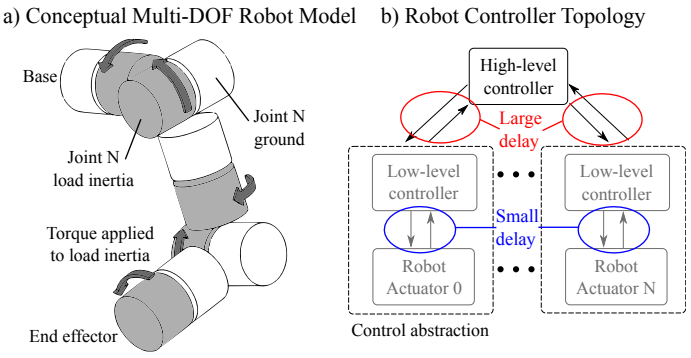

FIGURE 1. **Hypothetical Robot with a Distributed Controller.** Many highly articulated robots today use embedded systems collocated at each actuator to perform joint control. Reference trajectories are often passed from a central high-level controller to the distributed low-level controllers. The low-level controllers lack complete system knowledge, but are able to operate with extremely low delay compared to the high-level controller. This reduction in delay can benefit the closed-loop stability for high impedance joint control as explored in this paper.

as damaged nuclear reactor plants and actively perform tasks to mitigate damage and threat to human life [2]. The requirements for this competition spawned a number of complex robot designs which were intended to approach human levels of dexterity and strength, in order to improve surveillance coverage and enable proactive action by future robotic rescue workers. The increase in task complexity has therefore increased the complexity of robots designed to perform these tasks. For example, Valkyrie, NASA-JSC's entry into the DRC is a humanoid robot with 44 actuated Degrees-Of-Freedom (DOFs) [3].

As a result of this increased robot complexity and in contrast to many older, more conventional robots, new approaches have been required for communicating with and controlling so many coupled and coordinated actuators. Often, these communication approaches manifest themselves in a hierarchical control framework where a multi-joint controller delegates tasks to subordinate single-joint controllers (see Figure 1.) These single-joint controllers are often embedded directly into the robot's joints, collocating them with the actuation hardware. As a result, communication between actuator and the single-joint controller can occur a very high rates, while communication between single- and multi-joint controllers occurs more slowly (up to 10s of milliseconds).

Because of this separation of controllers, it is important to consider where, physically, a controller is being run when designing the closed-loop system. In this paper, we consider this physical separation of control, which we represent as a discrepancy in feedback latency seen by each type (multi- or single-joint) of controller. We therefore study the effect this latency has on the closed-loop system performance. We find that feedback relating to joint velocity is far more sensitive to latency than is stiffness feedback. This discovery motivates the idea of embedded damping, a control approach where damping feedback is implemented locally at the single-joint level while stiffness feedback occurs at the multi-joint level. The benefit of this split proportional-derivative impedance control approach over a monolithic impedance controller implemented at the multi-joint level is increased control loop stability due to the reduced damping feedback latency. As a direct result of this increased stability, feedback effort and thus closed-loop actuator impedance may be increased beyond the levels possible for a monolithic impedance controller. High impedance is desirable to minimize tracking error in the presence of disturbances.

While we propose implementing damping feedback at the joint level, we argue that it is beneficial to maintain stiffness feedback at the multi-joint level. The reasons for separation are two-fold. First, as we show in Section 2, closed-loop stability is far less dependent on stiffness latency than damping latency. Second, a richer assortment of control methods are made available by making the multi-joint controller aware of joint positions. For example, consider the case where joint-level controllers possess a full impedance controller and desired positions are passed to them from a multi-joint controller. For Cartesian position control of the end-effector the multi-joint controller must perform an inverse kinematic transformation from Cartesian space to joint space. Such a transformation is possible in some simple cases, such as in non-redundant robots. However, as the topology and number of tasks becomes more complex, obtaining absolute joint positions from a collection of desired task output positions becomes more difficult.

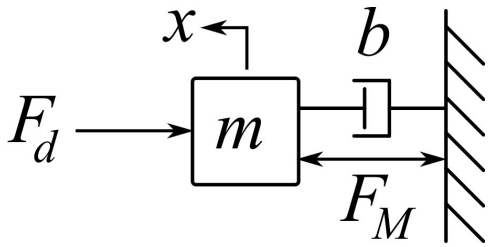

FIGURE 2. **Actuator and Control Plant Model.** This diagram represents a generalization of rigid actuators considered in this paper. F_M is the applied motor force, x is the load displacement output, m is effective output inertia, b is the actuator's passive damping, and F_d is an external disturbance force.

This problem has been solved using inverse kinematic Cartesian controllers [4] which use Jacobians to convert sensed Cartesian error into desired joint velocities. Such approaches require knowledge of end effector position at the multi-joint level which can be found using knowledge of individual joint positions.

The above example considers a goal of tracking end effector position, but a similar argument holds true for Cartesian impedance control goals. A Cartesian impedance control law implemented at the multi-joint level can be represented the summation of a proportional term and a derivative term based on Cartesian positions and generates a desired Cartesian force. This Cartesian force can then be translated into joint torques using the well-known Jacobians transpose relation. However, if directly implemented at the multi-joint level, the multi-joint controller requires the Cartesian velocity (derivative) variable. Because of this, the velocity data spans the multi-single joint domains and thus incurs large latencies, reducing stable gain magnitudes.

Following our proposed approach, we instead suggest implementing the proportional term at the multi-joint level and the derivative term at the single-joint level. As a result, feature-rich controllers are enabled by incorporating stiffness feedback at the multi-joint level while high gains are maintained by minimizing damping feedback latencies.

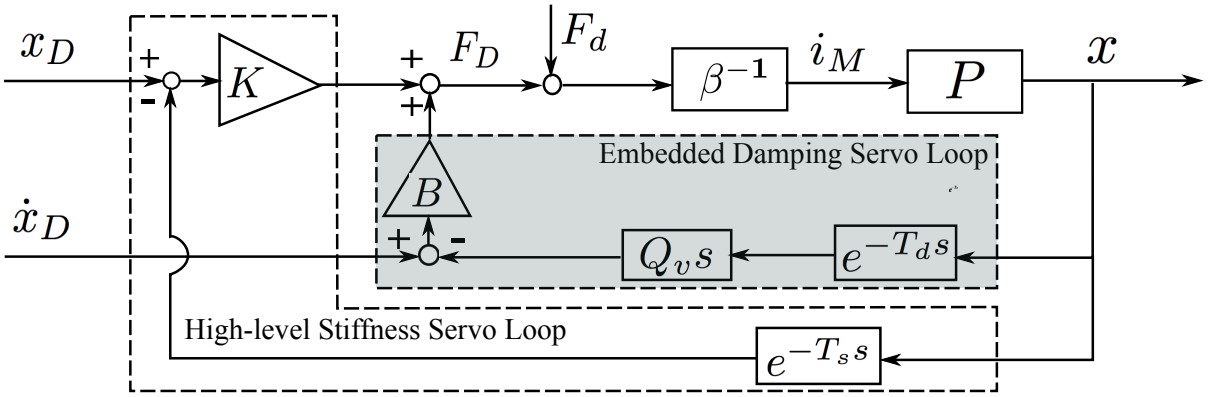

FIGURE 3. **Distributed Control Structure with Separate Stiffness and Damping Servos.** A simple proportional-derivative control law is used to control an actuator. P denotes the actuator plant with motor current input, i_M, and position output, x. β^{-1} represents a scaling constant mapping the desired force, F_D, to the motor current, i_M. K is the stiffness feedback gain while B is the damping feedback gain. The damping feedback loop is labeled as embedded to emphasize that it is meant to be locally implemented to take advantage of high servo rates. On the other hand the stiffness feedback is implemented in a high-level computational process close to external sensors, for instance. An external disturbance is denoted as F_d inserted between the controller and plant block as suggested by [5]. This disturbance is used to model load gravity in Section 3. Here, no force feedback is employed.

RELATED WORK

The effects of latency have often been studied recent years, especially in the work of regarding PID controller tuning [6, 7, 8, 9]. More recent work in this area also addresses velocity filtering, but assumes that an integral control parameter is available, thus making the work less directly applicable to impedance control scenarios [10].

The haptics community has also considered delay and filtering issues in impedance feedback control systems. Due to the destabilizing effects of these practical phenomena, significant effort has been put forth in ensuring systems are stable by restricting them to meet passivity criteria [11]. Other work relaxes these constraints and simply study how delay and filtering affects a true or false stability criteria [12, 13, 14, 15]. Detailed work has also been performed considering additional real-world effects such as quantization and coulomb friction on system stability [16].

In contrast to the aforementioned work, the work presented here considers the special case where delay between stiffness feedback and damping feedback is *different*. By testing phase margin based stability, step response and tracking accuracy, we verify that system stability and performance are insensitive to stiffness feedback delays compared with its damping feedback delays. Moreover, this scenario not only offers insight into impedance controller sensitivity, but also may be leveraged on many practical systems to improve disturbance rejection by increasing gains without compromising overall controller capability. As such, we expect these findings to be immediately useful on many complex robotic systems such as humanoid robotics among others.

Our long term goal is to design an unified decentralized cascaded control structure [17] applicable to humanoid robots. Cascaded control is not only capable of analyzing multiple feedback loops in a unified manner [18], but also is effective in reducing the number of system variables. This will play important roles in reducing the complexity of multiple-input multiple-output (MIMO) control systems. Finally, we aim at maximizing the impedance range of legged robots based on the constraints of feedback loop latencies, signal filtering and inherent system properties.

1 DISTRIBUTED IMPEDANCE CONTROL STRUCTURE

Rigid actuators can be approximately modeled as a force acting on a viscous inertia (Figure 2),

$$P(s) = \frac{x(s)}{F_M(s)} = \frac{1}{ms^2 + bs}. \tag{1}$$

Considering a current controlled motor, motor force (F_M) may be mapped into motor current (i_M) using

$$\beta = \frac{F_M}{i_M} = \eta N k_\tau. \tag{2}$$

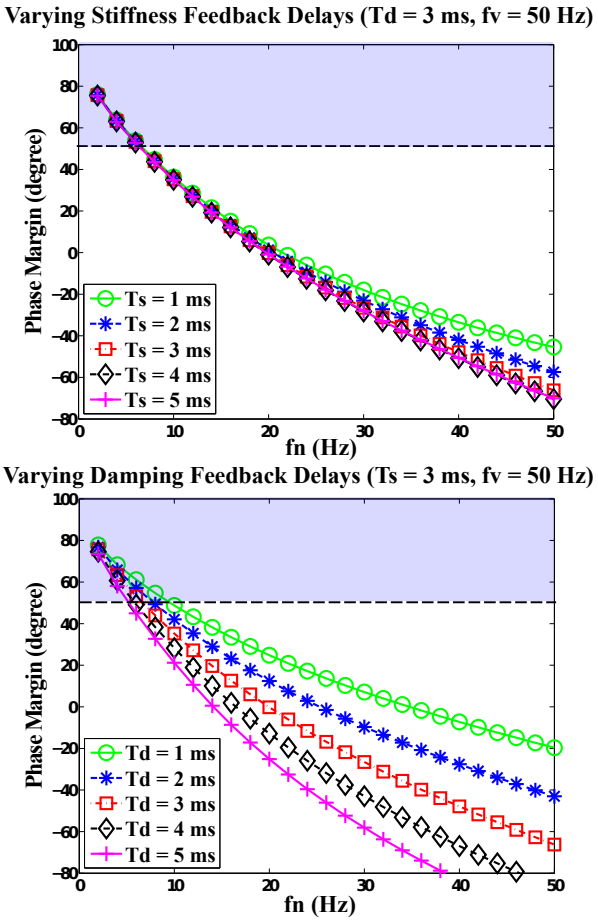

FIGURE 4. Simulation of Phase Margin Sensitivity to Stiffness and Damping Feedback Delays. Figures here show the phase margin sensitivity results with respect to a set of stiffness and damping feedback delays. The blue shaded region corresponds to a desired area where systems exhibit a non-oscillatory step response. It has a threshold phase margin of 50° [19]. The red lines with square markers in both figures are a reference line (i.e., $T_s = T_d = 3$ ms). T_s or T_d varies 1 ms each time. It can be seen that phase margin is more sensitive, i.e., larger variation, to damping feedback delays. Other system parameters include: filter cut-off frequency $f_v = 50Hz$, passive system mass $m = 256$ kg, passive damping $b = 1250$ Ns/m and damping ratio $\zeta_d = 1$.

Then, the control plant from i_M to x is

$$P(s) = \frac{x(s)}{F_M(s)}\frac{F_M(s)}{i_M(s)} = \frac{x(s)}{i_M(s)} = \frac{\beta}{ms^2+bs}. \quad (3)$$

Figure 3 shows a typical impedance control block including damping feedback filtering ($Q_v s$), stiffness feedback delay (T_s), damping feedback delay (T_d), stiffness feedback gain (K) and damping feedback gain (B). For such a control structure, desired motor force (F_D) is calculated as

$$F_D(s) = K(x_D - e^{-T_s s}x) + B(x_D s - e^{-T_d s}Q_v x s), \quad (4)$$

where x_D and $\dot{x}_D$ (i.e., $x_D s$) are the desired position and velocity respectively, and $F_M = F_D + F_d$ where F_d is a disturbance force. $e^{-T_s s}$ and $e^{-T_d s}$ represent time delay (i.e., latency) in the stiffness and damping feedback loop, respectively. In this paper, we assume the terminology "stiffness" is same as "position" or "proportional" while "damping" is same as "velocity" or "derivative". Using $P(s)$ in Equation (3), we can find the closed-loop transfer function $P_{CL}(s)$ from desired position (x_D) to load position (x)

$$P_{CL}(s) = \frac{x(s)}{x_D(s)} = \frac{Bs+K}{ms^2+(b+e^{-T_d s}BQ_v)s+e^{-T_s s}K}, \quad (5)$$

where Q_v is a first order low pass filter with cut-off frequency f_v

$$Q_v(s) = \frac{2\pi f_v}{s+2\pi f_v}. \quad (6)$$

The transfer function $P_{CL}(s)$ has a third order due to Q_v being a first order transfer function. This transfer function is similar to the one used in [19], except the difference in stiffness and damping feedback delays.

The main focus of this paper is to analyze the quantitative stability (i.e, using phase margins as a metric) and tracking performance of this closed-loop system with an emphasis on the impact of the various feedback delays, T_s and T_d. To this end, we will demonstrate how crucial it is to minimize damping feedback delay in terms of system stability, step response and tracking accuracy.

Before studying system sensitivity to various delays, we first design a gain selection criterion based on the denominator characteristic polynomial of Equation (5). In selecting gains, we disregard the filtering and feedback delay terms. A critically-damped step response $\zeta = 1$ is chosen as the desired performance. Comparing with a standard second order characteristic polynomial $s^2 + 2\zeta\omega_n s + \omega_n^2$, we have the following critically-damped gain equations:

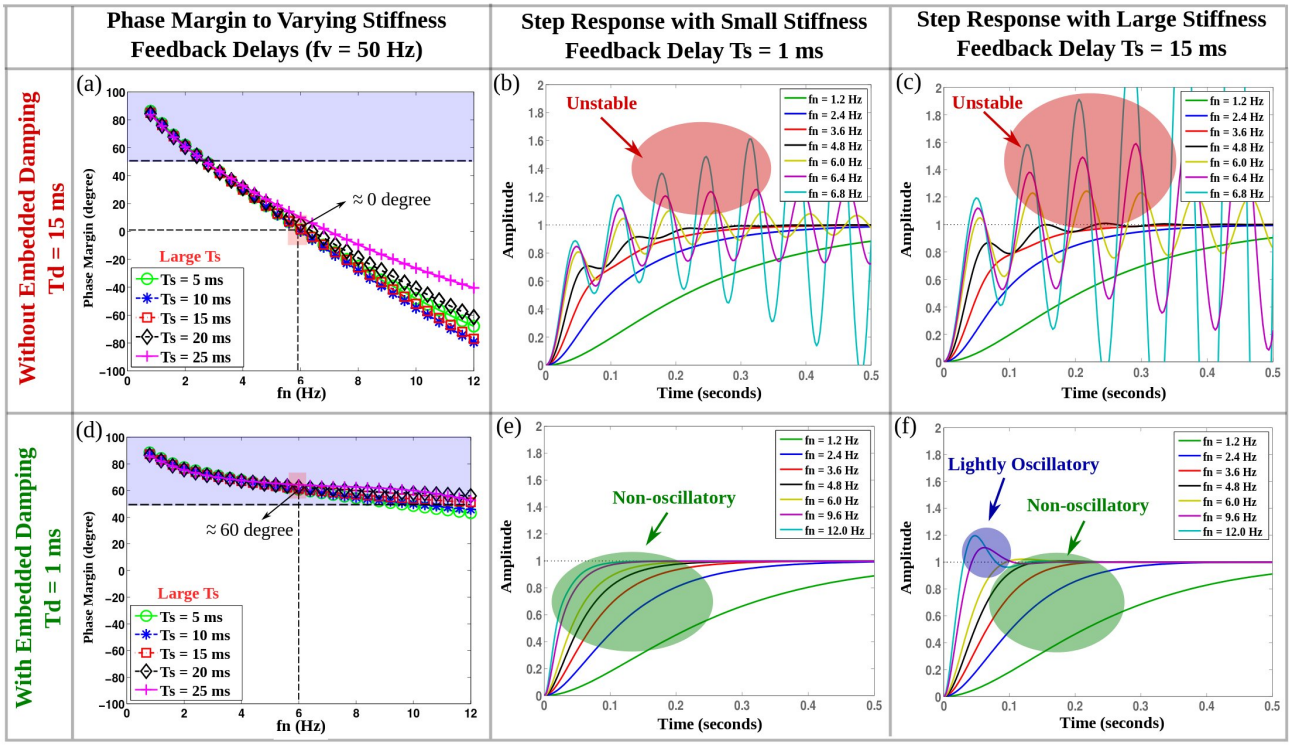

FIGURE 5. **Simulation of Step Response With and Without Embedded Damping.** Compared with figure (a), figure (d) has an embedded damping term with loop delay $T_d = 1$ ms. The phase margin is largely improved and most of the points remain within the blue region ($> 50^\circ$ phase margin). Phase margin insensitivity to stiffness feedback delays is also verified in (a) and (d). Step responses are illustrated in the remaining subfigures. As shown in figure (b), system response starts to show undesired oscillation at $f_n = 4.8$ Hz and almost sustained oscillation at $f_n = 6$ Hz. At frequency higher than $f_n = 6$ Hz, the system becomes unstable. If we increase the stiffness feedback delay to $15ms$ in subfigure (c), the step response is almost identical with a slight distortion. In the embedded damping case, the system appears to be critically-damped until $f_n = 12$ Hz in subfigure (e). When we increase the stiffness feedback delay to 15 ms in subfigure (f), the system responses from 7.2 Hz to 12 Hz show an overshoot but converge to steady state within 0.2 seconds. Comparing subfigures (b) and (e), we can conclude that lowering damping feedback delay is more dominant in affecting system performance, although lowering stiffness feedback delay gives the benefit to some degree.

$$
\begin{aligned}
K &= m\omega_n^2, \\
B &= 2\zeta\sqrt{mK} - b, (\zeta = 1) \\
f_n &= \frac{\omega_n}{2\pi} = \frac{1}{2\pi}\sqrt{\frac{K}{m}}.
\end{aligned} \tag{7}
$$

The natural frequency (f_n) has a monotonic relationship with our controller gains. Note that, the main purpose of this gain selection rule is to make K and B dependent on each other, as is done in [19]. Critically-damped performance can not be guaranteed due to feedback delay and signal filtering. On the contrary, as we show in the following section, a phase margin based method can be used to study how the complete system reacts to signal filtering and feedback delay.

2 PHASE MARGIN SENSITIVITY COMPARISON

In this section, the utility of embedded damping (i.e., small damping feedback delay) is demonstrated by the study of phase margin and step response sensitivity with respect to stiffness and damping feedback delays. The transfer function used in this section is $P_{CL}(s)$ in Equation (5). First, the phase margin sensitivity is studied by two delay sampling ranges: one is small range with $1-5$ ms in Figure 4 while the other one is $5-25$ ms in Figure 5 (a) and (d). These delays roughly correspond to those found in highly complex robots due to contributions from low level actuation, sensing layers and high level planning and control layers [3]. The results show that the phase margin is more sensitive to the damping feedback delay T_d compared with its stiffness counterpart T_s. When faced with the choice of lowering either T_s or T_d, based on the results shown in Figure 5, it is evident that T_d is far more sensitive to increased delay and thus should be minimized

with high priority.

Several observations are taken from the results shown in Figure 5. First, reducing the damping feedback delay plays a dominant role in improving the system phase margin and step response performance. Comparing Figure 5 (a) and (d), the damping feedback delay reduction boosts phase margin dramatically. This also can be verified by the second subfigure in Figure 4. The step responses in Figure 5 (b) and (e) (or (c) and (f)) show that reducing T_d from 15 ms to 1 ms dramatically reduces oscillation for the same natural frequency f_n. These results emphasize the significance of implementing the damping term at the fastest control loop to keep the damping feedback delay as small as possible.

Second, the phase margin and step response are insensitive to stiffness feedback delays. Phase margin values in either Figure 5 (a) or (d) vary within a relatively small region when only T_s varies. Trivial variations of step responses to T_s also can be checked by comparing Figure 5 (b) and (c) (or (e) and (f)) respectively.

Third, Figure 4 (a) and Figure 5 (a) seem to indicate that increasing T_s actually increases the phase margin for some values of f_n. This is counterintuitive. To confirm this observation we obtain a Nichols diagram [5] from the open-loop transfer function. Equation (5) can be rewritten as

$$P_{CL}(s) = \frac{\frac{Bs+K}{ms^2+bs}}{1+\frac{e^{-T_d s}BQ_v s+e^{-T_s s}K}{ms^2+bs}} = \frac{\frac{Bs+K}{ms^2+bs}}{1+P_{OL}(s)}, \tag{8}$$

where $P_{OL}(s) \triangleq P(s)H(s)$ is the open loop transfer function according to [5], $P(s)$ is the system's plant, and $H(s)$ is the so-called feedback transfer function. Thus, we have

$$P_{OL}(s) = \frac{e^{-T_d s}BQ_v s + e^{-T_s s}K}{ms^2+bs}. \tag{9}$$

Using this $P_{OL}(s)$, the Nichols diagram is shown in Figure 6. The top diagram confirms this inconsistency because the curves flip at the value of 0 dB.

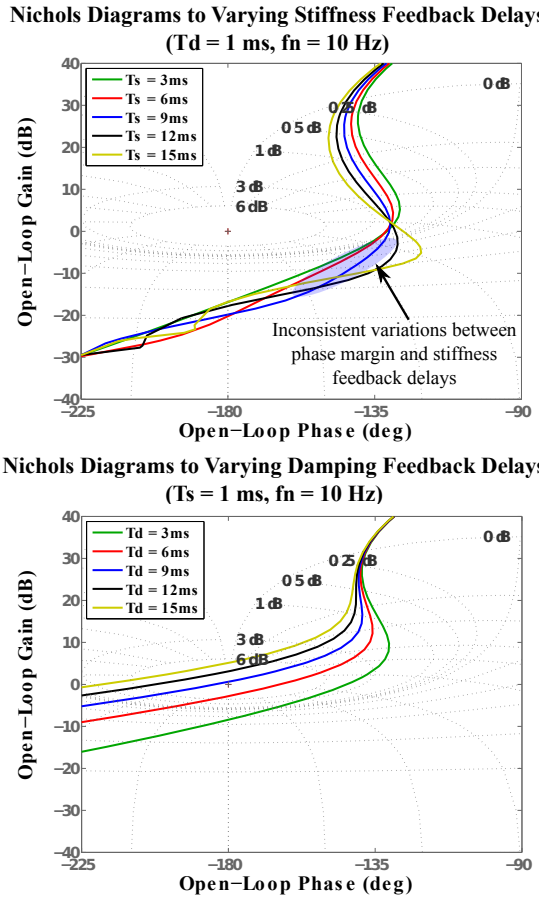

FIGURE 6. **Nichols Diagrams to Varying Feedback Delays.** The open loop transfer function $P_{OL}(s)$ is used to generate the Nichols diagrams. Comparing these two subfigures, we can conclude that phase margin doesn't have a consistent relationship with stiffness feedback delays.

3 EVALUATION OF DISTRIBUTED CONTROLLER UNDER DISTURBANCES

This section presents a case study of tracking performance of a humanoid robot knee joint when experiencing two different external gravitational disturbances. We present this study as a means of demonstrating how the implementation of an embedded damping term may benefit system level performance.

First, two sets of knee joint trajectories are generated by a multiple-step walking motion planner [20]. Here, we emulate two legged robot scenarios: one is a fast leg swing motion with a small load (e.g., shank load) while the second is a slow leg stance motion with a large upper body load (i.e., effective whole body load on knee). In this simulation, it is assumed that the fast motion has a peak angular velocity $\dot{\theta}_{max} = 6$ m/s while the slow trajectory has $\dot{\theta}_{max} = 2.5$ rad/s. These two types of trajectories are applied to simulations of NASA-JSC's Valkyrie robot knee actuator using the configurations shown Table 1.

The external gravity load is modeled as a constant disturbance F_d. Thus, the desired command becomes

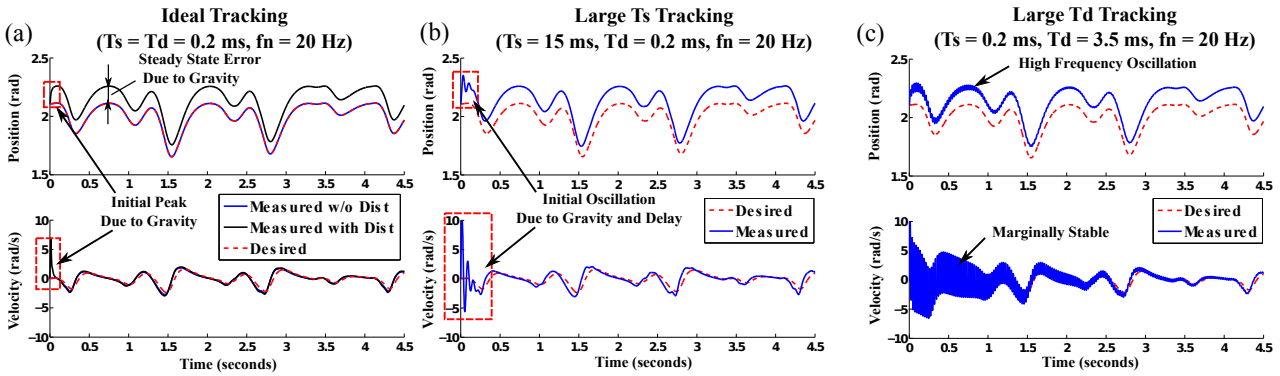

FIGURE 7. **Simulation of Stiffness and Damping Feedback Delay Tolerance of Valkyrie Joint Tracking under Disturbance.** Subfigure (a) shows an ideal tracking case when both stiffness and damping feedback delays are 0.2 ms. In Valkyrie, feedback delay at low-level is around 0.2 ms. When no disturbance is applied, the blue measured data accurately tracks the red desired data. When a disturbance force F_d is applied (black line), position tracking shows a sustained offset while velocity tracking maintains accurate tracking with a slight error by inspection. In subfigures (b) and (c), we verify how large stiffness or damping feedback delays the system can tolerate before going unstable. Subfigure (b) shows that system remains stable until $T_s = 15$ ms when $T_d = 0.2$ ms. However, in subfigure (c), system already becomes marginally stable when T_d increases to 3.5 ms. These results validate our conclusion in Section 2 that system stability is more sensitive to damping feedback delays than stiffness feedback delays. Note that we could further reduce the offset error in position tracking by increasing controller gains. In that case, small oscillations will show up along the trajectory.

TABLE 1. Valkyrie Knee Actuator Parameters

Parameters	Swing Phase	Stance Phase
Stiffness Delay T_s	15 ms	15 ms
Damping Delay T_d	0.2 ms	0.2 ms
Disturbance Force F_d	2000 N	8000 N
Maximum Joint Speed θ_{max}	6 rad/s	2.5 rad/s

$$F_D = m\ddot{x} + b\dot{x} - F_d. \tag{10}$$

Note that F_d is a linear force mapped from the torque due to gravity. In fact, there could be other types of disturbances, such as external impact force. Our case only considers the gravity term since it is a dominant factor that we found critically influences Valkyrie's locomotion stability and performance during our involvement in the DARPA Robotics Challenge Trials 2013.

We can derive the disturbance transfer function from Figure 3

$$P_d(s) = \frac{x(s)}{F_d(s)} = \frac{1}{ms^2 + (b + e^{-T_d s}BQ_v)s + e^{-T_s s}K}, \tag{11}$$

which has the same denominator characteristic polynomial as Equation (5). Thus, the critically-damped gain selection rule also applies to the disturbance case. Although the non-zero property will change the transient dynamics to some degree, the inherent system property remains invariant in terms of stability. As shown in Equation (11), given a constant F_d, the higher controller gains are, the smaller x is, meaning the influence on the output position is reduced. Namely, higher K and B increases actuator stiffness and reduces the position error induced by disturbances. Thus, our strategy for disturbance rejection is to implement high controller gains as much as possible while obeying the critically-damped selection rule. The gravitational load is taken as a disturbance instead of compensating for it in a feedforward manner.

We first evaluate a moderate speed joint motion with a very large inertia and heavy gravitational load induced by the whole-body weight. Valkyrie has an effective weight of 1300 N on the knee and a thigh length of 0.37 m. When the knee flexes 25°, the gravity torque on the knee is approximately $\tau_g = m_c \cdot g \cdot l_c \cdot sin\theta_k \approx 1300 * 0.37 * sin(0.43) = 200$ Nm where m_c is the mass of the whole body, gravity acceleration constant $g = 9.8$ m/s^2, the distance between the whole body center of mass and the knee joint axis is $l_c = 0.37$ m and the bent knee angle $\theta_k = 25°$. Since the knee lever arm $r \approx 0.025$ m, $F_d = \tau_g/r = 200/0.025 = 8000$ N, which is the disturbance force in stance phase of Table 1. Similarly, three different scenarios are simulated in Figure 7. Note that, the radius r should be joint angle dependent but vary within a small range. Thus, we assume it to be constant for simplicity.

We then evaluate a fast joint motion with a relatively small in-

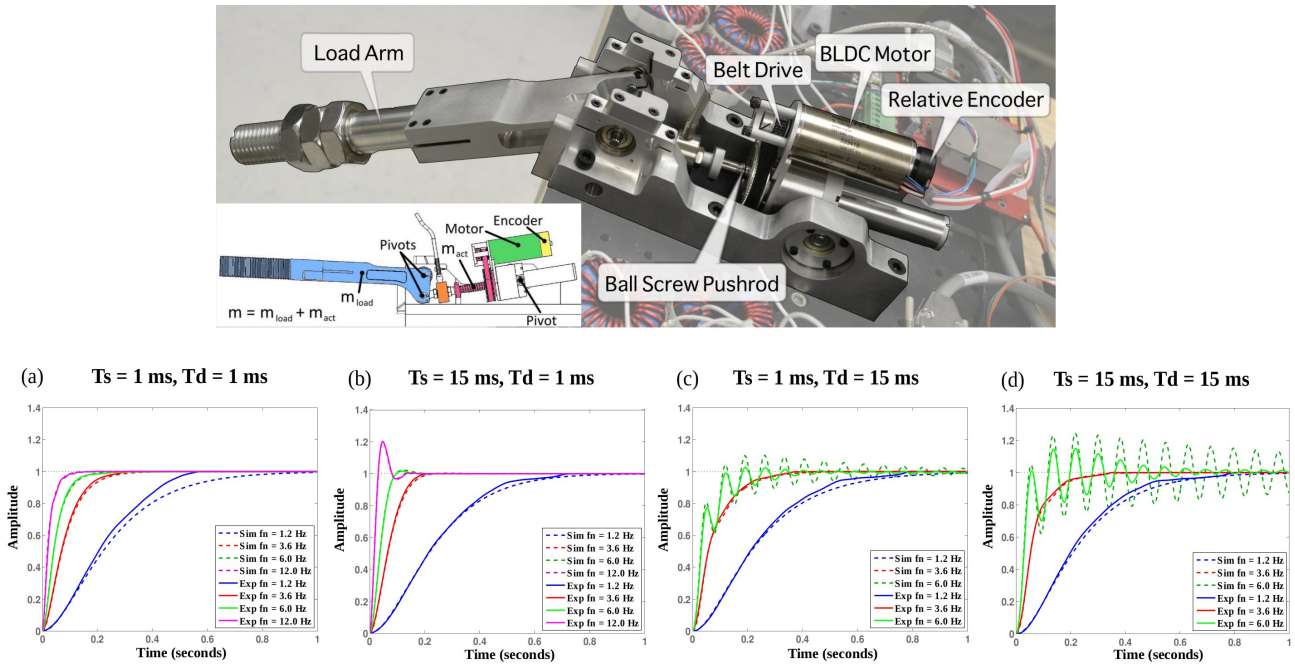

FIGURE 8. **Step Response Experiment with Distributed Controller.** Subfigures (a) through (d) show various implementations on the UT linear rigid actuator above of the simulations depicted on Figure 5. Overlapped with the data plots, exact simulations of the experiments are also shown. The experiments not only confirm the higher sensitivity of the actuator to damping than to stiffness delays but also indicate a good correlation between the real actuator and the simulations.

ertia, emulating knee action on Valkyrie's leg during swinging motion. To simulate this scenario, the leg's shank parameters is used to estimate the gravity torque, $\tau_g = m_s \cdot g \cdot l_s \cdot sin\theta_k \approx 20 \cdot 9.8 \cdot 0.25 \cdot sin(1.57) = 50$ Nm where the mass of the shank is $m_s = 20$ kg, gravity acceleration constant $g = 9.8$ m/s^2, the distance between the shank's center of mass and the knee joint axis is $l_s = 0.25$ m and the fully bent knee angle $\theta_k = 1.57$ rad. Thus the estimated linear force $F_d = 50/0.025 = 2000$ N. This value corresponds to the disturbance force in swing phase of Table 1. Based on this F_d and feedback delays in Table 1, we carry out simulations for three different cases in Figure 9.

4 EXPERIMENTAL VALIDATION

This section provides experimental results that validate our theoretical and simulation results. Step responses with different feedback delays are implemented on the actuator in Figure 8. They validate transient dynamics and stability sensitivity to stiffness and damping feedback delays. The results in Figure 8 show a close match between simulations and experiments. For consistency, the experiment uses the same stiffness and damping feedback delays that are used in Figure 5. In the quasi-critically damped cases, the experiments and simulations achieve almost identical results. In the underdamped cases, the experimental results show less oscillation compared to the simulations. This discrepancy may be caused by Coulomb friction and unmodeled drive train dynamics. We also tested the step response with a 2.25 kg weight. However, this extra weight aggravated the influence of a small amount of backlash, which deteriorated the tracking performance dramatically.

5 DISCUSSION AND CONCLUSION

There are several directions we intend to explore in future work. First, we plan to implement more simulation scenarios presented on the rigid actuator hardware platform in Figure 8. Second, in Figure 3, we have not yet added a feedforward acceleration term to commanded force F_D. However, preliminary simulation results show that this acceleration contributes little to the tracking accuracy due to its extremely small value compared to the proportional-derivative terms. It is because our strategy is to maximize impedance gains for high stiffness performance and the commanded force heavily relies on feedback control instead of the model based feedforward term. Thus, impedance control dominates the value of F_D. In the future we will study more about the model-based control where control effort will contribute more from feedforward terms. Third, we are exploring the critically-damped gain selection rule for series elastic actu-

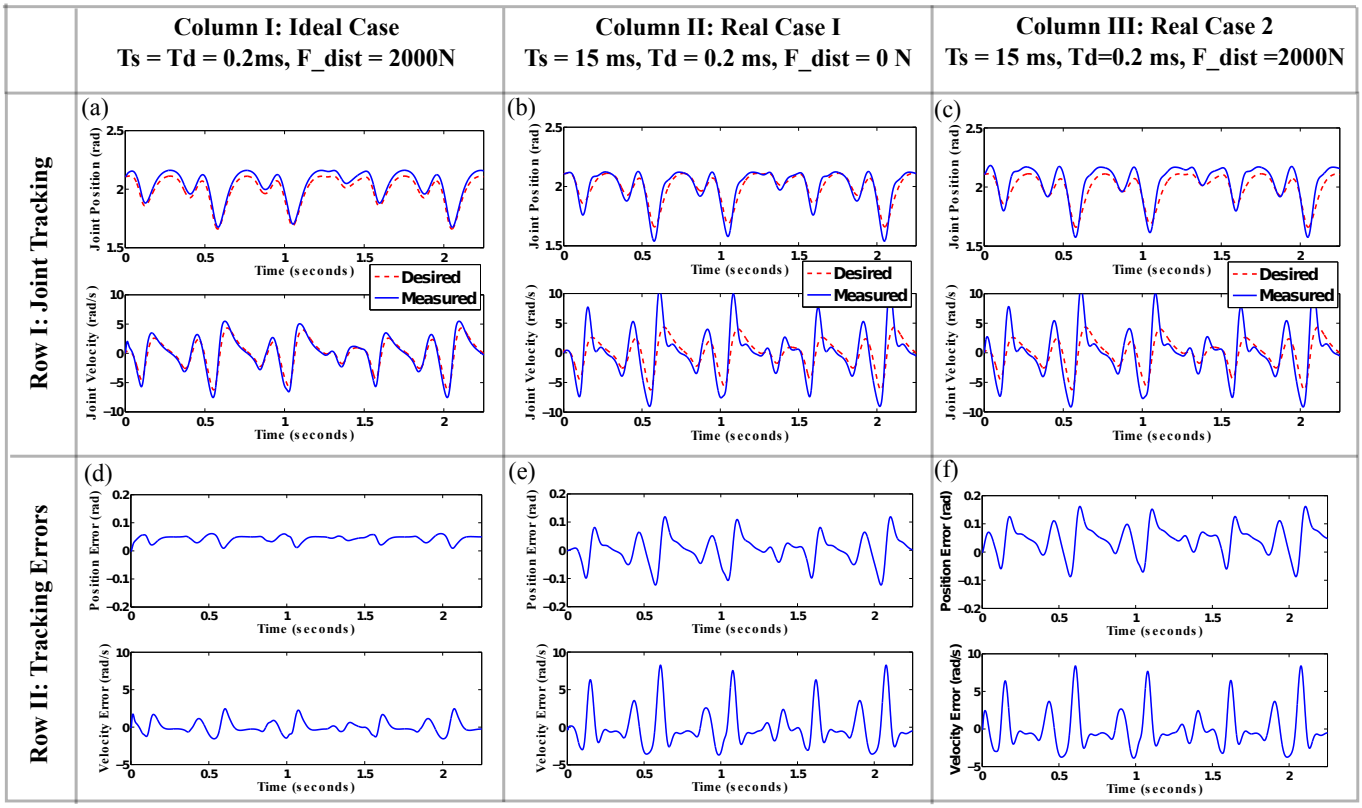

FIGURE 9. **Simulation of Fast Swing Joint Tracking With/Without Embedded Damping and Disturbance.** In this figure, each column represents a specific case in terms of feedback delays and gravitational disturbance. Column I: when feedback delays are small, the position and velocity tracking are quite accurate. Position tracking shows around 1° peak error while velocity tracking has 2.5 rad/s peak error. As a result, the 2000 N gravitational disturbance does not largely deteriorate the tracking performance. Column II: when feedback delay $T_s = 15$ ms, $T_d = 0.2$ ms is considered, both position and velocity tracking errors dramatically increase. Column III: this case has both $T_s = 15$ ms, $T_d = 0.2$ ms feedback delays and 2000 N gravitational disturbance. As figure shows, the tracking accuracy is similar to that in Column II. This means our controller can tolerate large gravitational disturbance with small errors if high controller gains (i.e., high f_n) are employed. Comparing Columns I and II, we conclude that feedback delays play dominant roles in position and velocity tracking accuracy. This is consistent with our conclusion on delays in Section 2.

ators (SEA) with inner torque feedback loop. Then the system will become a fourth order system with feedback delays and filtering. We plan to characterize that system by a multiplication of two standard second order systems. Fourth, we are also targeting to find an SEA optimal analytical relationship between $f_{n_{max}} = f(f_p, K_x, K_\tau, T_x, T_\tau, f_v)$ where $f_{n_{max}}$ represents the maximum natural frequency which guarantees critically-damped response, f_p is passive corner frequency. K_x and K_τ are the gain sets for stiffness feedback and torque loop, respectively. T_x and T_τ are the stiffness and torque feedback delays, respectively. A sampling based optimization algorithm could be implemented to achieve the maximum impedance range (i.e., Z-width).

In this paper, the effects of stiffness and damping feedback latencies on closed-loop system stability are demonstrated by studying phase margin based stability, step response performance and tracking accuracy. Our simulations are tested based on a rigid actuator with an impedance controller. We verify that system stability and performance are more sensitive to the damping feedback delays than stiffness feedback delay. Trajectory tracking accuracy with gravitational disturbance is tested by emulating a fast swing and a slow stance motion of NASA-JSC's Valkyrie legged robot. The experimental results validate the high sensitivity of damping feedback delays and the significance of implementing embedded damping.

REFERENCES

[1] Nagatani, K., Kiribayashi, S., Okada, Y., Otake, K., Yoshida, K., Tadokoro, S., Nishimura, T., Yoshida, T., Koyanagi, E., Fukushima, M., and Kawatsuma, S., 2013. "Emergency response to the nuclear accident at the Fukushima Daiichi Nuclear Power Plants using mobile rescue robots". *Journal of Field Robotics,* ***30***(1), pp. 44–63.

[2] DARPA, 2014. The DARPA robotics challenge. http://www.theroboticschallenge.org. Accessed: 2014-02-27.

[3] Paine, N., Mehling, J., Holley, J., Radford, N., Johnson, G., Fok, C., and Sentis, L. "Actuator Control for the NASA-JSC Valkyrie Humanoid Robot: A Decoupled Dynamics Approach for Torque Control of Series Elastic Robots". *Journal of Field Robotics (Submitted 2014)*.

[4] Sentis, L., Park, J., and Khatib, O., 2010. "Compliant control of multi-contact and center of mass behaviors in humanoid robots". pp. 483–501.

[5] Ogata, K., and Yang, Y., 2010. "Modern control engineering".

[6] Åström, K. J., 1993. "Automatic tuning and adaptation for PID controllers - A survey". *Control Eng. Practice,* ***1***, pp. 699–714.

[7] Lee, C.-H., 2004. "A survey of PID controller design based on gain and phase margins". *International Journal of Computational Cognition,* ***2***, pp. 63–100.

[8] Poulin, E., Pomerleau, A., Desbiens, A., and Hodouin, D., 1996. "Development and evaluation of an auto-tuning and adaptive PID controller". *Automatica,* ***32***(1), pp. 71–82.

[9] W. K. Ho, K. W. L., and Xu, W., 1998. "Optimal gain and phase margin tuning for PID controllers". *Automatica,* ***34***(8), pp. 1009–1014.

[10] Åström, K. J., Panagopoulos, H., and Hägglund, T., 1998. "Design of PI controllers based on non-convex optimization". *Automatica,* ***34***(5), May, pp. 585–601.

[11] Colgate, J., and Schenkel, G., 1994. "Passivity of a class of sampled-data systems: Application to haptic interfaces". In American Control Conference, Vol. 3, pp. 3236–3240.

[12] Lawrence, D., 1988. "Impedance control stability properties in common implementations". In Robotics and Automation, Proceedings., IEEE International Conference on, Vol. 2, pp. 1185–1190.

[13] Colgate, J., and Brown, J., 1994. "Factors affecting the Z-Width of a haptic display". In Robotics and Automation, Proceedings., IEEE International Conference on, Vol. 4, pp. 3205–3210.

[14] Mehling, J., Colgate, J., and Peshkin, M., 2005. "Increasing the impedance range of a haptic display by adding electrical damping". In Eurohaptics Conference, Symposium on Haptic Interfaces for Virtual Environment and Teleoperator Systems, pp. 257–262.

[15] Hulin, T., Camarero, R. G., and Albu-Schaffer, A., 2013. "Optimal control for haptic rendering: Fast energy dissipation and minimum overshoot". In Intelligent Robots and Systems (IROS), 2013 IEEE/RSJ International Conference on, IEEE, pp. 4505–4511.

[16] Diolaiti, N., Niemeyer, G., Barbagli, F., and Salisbury, J., 2006. "Stability of haptic rendering: Discretization, quantization, time delay, and coulomb effects". *Robotics, IEEE Transactions on,* ***22***(2), April, pp. 256–268.

[17] Vallery, H., Veneman, J., Van Asseldonk, E., Ekkelenkamp, R., Buss, M., and Van Der Kooij, H., 2008. "Compliant actuation of rehabilitation robots". *Robotics & Automation Magazine, IEEE,* ***15***(3), pp. 60–69.

[18] Mosadeghzad, M., Medrano-Cerda, G. A., Saglia, J. A., Tsagarakis, N. G., and Caldwell, D. G., 2012. "Comparison of various active impedance control approaches, modeling, implementation, passivity, stability and trade-offs". In Advanced Intelligent Mechatronics (AIM), 2012 IEEE/ASME International Conference on, IEEE, pp. 342–348.

[19] Paine, N., and Sentis, L., 2014. "A closed-form solution for selecting maximum critically damped actuator impedance parameters". In ASME Journal of Dynamic Systems, Measurement, and Control, ASME, In Press.

[20] Zhao, Y., and Sentis, L., 2012. "A three dimensional foot placement planner for locomotion in very rough terrains". In Humanoid Robots (Humanoids), 2012 12th IEEE-RAS International Conference on, IEEE, pp. 726–733.